Rüffel, V., Maar, M., Dammbrück, M.N., Hauröder, B., **Neu, T.R.**, Meier, J. (2018):
Thermodesulfobium sp. strain 3baa, an acidophilic sulfate reducing bacterium forming biofilms triggered by mineral precipitation
Environ. Microbiol. **20** (10), 3717 - 3731

Thermodesulfobium sp. strain 3baa, an acidophilic sulfate reducing bacterium forming biofilms triggered by mineral precipitation

Authors and affiliations

Viola Rüffel,[1] Mona Maar,[1] Markus N. Dammbrück,[1] Bärbel Hauröder,[2] Thomas R. Neu,[3] Jutta Meier[1]*

[1] Institute for Integrated Natural Sciences, University Koblenz-Landau, 56070 Koblenz, Germany

[2] Bundeswehr Central Hospital Coblenz, Department of Pathology, Electron Microscopy, 56070 Koblenz, Germany

[3] Helmholtz Centre of Environmental Research – UFZ, Department of River Ecology, 39114 Magdeburg, Germany

Corresponding author*

Dr. Jutta Meier

Institute for Integrated Natural Sciences

University Koblenz-Landau

Universitätsstr. 1

56070 Koblenz

Germany

E-Mail: jmeier@uni-koblenz.de

Tel.: +49-261-2872227

Fax: +49-261-287-100-2227

This article has been accepted for publication and undergone full peer review but has not been through the copyediting, typesetting, pagination and proofreading process, which may lead to differences between this version and the Version of Record. Please cite this article as doi: 10.1111/1462-2920.14374

Running title

Acidophilic sulfate reducer forming biofilms

Originality-Significance Statement

Gene sequences of sulfate reducing bacteria affiliated with the genus *Thermodesulfobium* are often found in natural sulfuric environments making them prospective candidates for the remediation of acidic metal-rich waste water. In this study, we investigated a new acidophilic strain which we isolated from sediments of an acidic mine pit lake by applying a mineral medium containing inorganic ion concentrations similar to those of the pore water. By this means – in contrast to previous studies – natural buffering systems were used. The formation of Al hydroxides and Fe sulfides leads to a release of protons that counteracts proton consumption through sulfate reduction. We found evidence that suggests that mineral precipitation may have a positive effect on biofilm formation and consequently on sulfate reduction rates. Particularly Al hydroxides appeared to be a prerequisite for cell attachment to solid surfaces. Thereby they take over the function of extracellular polymeric substances that were apparently absent from the biofilm. To the best of our knowledge this is the first study to address biofilm growth and mineral formation with respect to sulfate reducing prokaryotes and their ability to grow at low pH levels. These processes most likely occur in the natural environment and are crucial for a successful treatment of waters affected by acid mine drainage.

Abstract

Sulfate reducing prokaryotes are promising candidates for the remediation of acidic metal-rich waste waters. However, only few acidophilic species have been described to date. Chemolithoautotrophic strain 3baa was isolated from sediments of an acidic mine pit lake. Based on its 16S-rRNA gene sequence it belongs to the genus *Thermodesulfobiu*m. It was identified as an acidophile growing in artificial pore water medium in the range of pH 2.6 – 6.6. Though the highest sulfate reduction rates were obtained at the lower end of this range, elongated cells and extended lag phases demonstrated acid stress. Sulfate reduction at low pH was accompanied by the formation of mineral precipitates strongly adhering to solid surfaces. A structural investigation by laser scanning microscopy, electron microscopy and X-ray microanalysis revealed the formation of Al hydroxides and Fe sulfides which were densely populated by cells. Al hydroxides precipitated first, enabling initial cell attachment. Colonization of solid surfaces coincided with increased sulfate reducing activity indicating more favorable growth conditions within biofilms compared to free-living cells. These findings point out the importance of cell-mineral interaction for biofilm formation and contribute to our understanding how sulfate reducing prokaryotes thrive in both natural and engineered systems at low pH.

Introduction

Sulfate reducing prokaryotes (SRP) are able to gain their energy by anaerobic respiration with sulfate as the terminal electron acceptor and hydrogen, low molecular weight fatty acids or alcohols as their most common electron donors (Barton & Fauque 2009, Rabus et al. 2013). Sulfate is reduced to hydrogen sulfide which is then released by the cell (Bradley et al. 2011, Rabus et al. 2013). The free sulfide species (H_2S/HS^-) may readily react with the

transition metal cations Mn^{2+}, Fe^{2+}, Co^{2+}, Ni^{2+}, Cu^{2+}, and Zn^{2+} to form complexes, clusters, and eventually solid phases (Rickard & Morse 2005, Rickard & Luther 2007). Depending on the electron donor and carbon source as well as the fate of metabolites, microbial sulfate reduction may lead to an increased pH level (Wendt-Potthoff & Neu 1998, Gallagher et al. 2012).

Hence, microbial sulfate reduction is highly useful for the treatment of acidic waters with high contents of dissolved metals and sulfate which are often caused by acid mine drainage (AMD). This process refers to the weathering of primary sulfide minerals as a consequence of coal and ore mining activities and the subsequent dissolution of carbonates and aluminosilicates by sulfuric acid (Blowes et al. 2003, Nordstrom 2011, Chen et al. 2016). Removal of the predominant metals from aqueous solution happens through the formation of either sulfides or, as in the case of Al^{3+}, hydroxides and hydroxysulfates due to an increase of pH (Furrer et al. 2002, Sánchez-España et al. 2016a, 2016b). Naturally occurring sulfate reduction has been identified as the most important process of alkalinity generation in lakes affected by AMD (Geller et al. 2013, Peiffer 2016) and has found wide application in active and passive treatment systems (Sheoran et al. 2010, Sánchez-Andrea et al. 2014). The operation of sulfidogenic bioreactors at low pH conditions and the selective removal of metals have been demonstrated in several studies (e.g. Bijmans et al. 2010, Ňancucheo & Johnson 2014, Fálagan et al. 2017).

Whether the role of SRP in the formation of (sulfide) minerals goes beyond the mere production of the reactant sulfide or the consumption of protons, is still under debate (Rickard & Morse 2005, Pósfai & Dunin-Borkowski 2006). In general, functional groups of cell wall polymers and extracellular polymeric substances (EPS) may interact with metal cations and provide mineral nucleation sites (Fortin & Beveridge 2000, Harrison et al. 2007,

Flemming et al. 2016). A close association of sulfide minerals with the EPS matrix was observed in naturally occurring biofilms (e.g. Moreau et al. 2007, MacLean 2008) and laboratory cultures (White and Gadd 1998, 2000). In addition, the formation of sulfides on the cell surface or within the cell envelope (e.g. Fortin et al. 1994, Donald & Southam 1999, Picard et al. 2018) would underline the important role of biopolymers in the formation of sulfides. The binding of Al^{3+} and the formation of Al hydroxides on cell surfaces in mixed or pure sulfate reducing cultures have been reported in several studies (Hard et al. 1999, Meier et al. 2012, Fálagan et al. 2017). Despite the wide application of sulfidogenic bioreactors for the treatment of AMD affected waters, only very few studies were directed to the biofilm formation and the interaction of cells with mineral precipitates (e.g. Koschorreck et al. 2010, Fálagan et al. 2017).

A high diversity of sulfate reducing bacteria was found in sulfidogenic bioreactors at low pH, however, not all members were considered to be acidophilic (reviewed in Sánchez-Andrea et al. 2014). Acidophiles are defined as organisms optimally growing within the pH range of 0.5 – 5 (Slonczewski et al. 2009). Only few acid tolerant or (moderate) acidophilic sulfate reducing species have been validly described so far. These include the mesophiles *Desulfosporosinus acidiphilus* (Alazard et al. 2010) and *Desulfosporosinus acididurans* (Sánchez-Andrea et al. 2015) as well as the thermophiles *Thermodesulfobium narugense* (Mori et al. 2003) and *Thermodesulfobium acidiphilum* (Frolov et al. 2017) within the Clostridia. For a putatively acid tolerant member of the Deltaproteobacteria, *Desulfovibrio* sp. TomC, the draft genome has been announced (Karnachuk et al. 2015a). Most attempts in cultivating SRPs within a mesophilic temperature range at low pH conditions using organic electron donors resulted in the isolation of *Desulfosporosinu*s spp. (e.g. Sen & Johnson 1999, Küsel et al. 2001, Senko et al. 2009, Karnachuk et al. 2015b). In contrast,

Thermosdesulfobium spp. were enriched with H_2 as electron donor partly outnumbering *Desulfosporosinus* spp. in the media set to lower pH values (Meier et al. 2012, Sánchez-Andrea et al. 2013).

To further explore acid tolerant or acidophilic sulfate reducers we aimed to obtain a pure culture using H_2/CO_2 as electron donor/carbon source and a mineral medium containing concentrations of the main inorganic ions corresponding to those of sediment pore waters of an acidic pit lake (Meier et al. 2012). In order to determine the pH range and the pH optimum of the successfully isolated strain, batch growth experiments were performed in the so-called artificial pore water medium (APWM) with the initial pH set to values in the range of pH 2 – 7. Furthermore, we were interested in the formation of Al and Fe precipitates and the role cell surfaces and possibly EPS may play in it. As the formation of precipitates strongly adhering to solid surfaces had been observed in media at low pH (pH 2.6 – 3.3), we conducted additional batch growth experiments in APWM set to pH 3 including removable carriers. In order to monitor biofilm and precipitate formation, these were visualized and analyzed by confocal laser scanning microscopy (CLSM), scanning (SEM) and transmission electron microscopy (TEM) accompanied by X-ray microanalysis.

Results

Growth characteristics of strain 3baa as a function of initial pH (pH_{ini} 2 – 7)

The pure culture of the designated strain 3baa grew within a range of pH_{ini} 2.6 – 6.6. Neither an increase in cell number nor a reduction of sulfate was observed at pH_{ini} 2.0 or pH_{ini} 6.9. The total amount of sulfate reduced during incubation was highest at pH_{ini} 2.6 – 4.2 (17$\pm$1 mmol l^{-1}) and lowest at pH_{ini} 6.6 (3 mmol l^{-1}) (Fig. 1A). The highest sulfate reduction rate (SRR) was observed at pH_{ini} 2.6 with a mean of 1.44 mM d^{-1} (Fig. 1A). In the range of pH_{ini} 3.1

– 5.6 similar rates of approximately 1 mM d^{-1} were determined. At higher initial pH values SRRs decreased markedly. Cell numbers obtained from the culture liquid at the end of incubation demonstrated highest yields in media set to intermediate pH values (Fig. 1B; pH_{ini} 4.2 – 5.6). Lowest final cell numbers were detected at pH_{ini} 2.6 – 3.3 which coincided with the formation of precipitates and/or biofilm on the walls of the serum bottles. Despite the high variation in cell counts, differences were significant (Kruskal-Wallis; $p < 0.05$) between intermediate (pH_{ini} 4.2 – 5.6) and low values (pH_{ini} 2.6 – 3.3) as well as pH_{ini} 6.6. A slight increase in pH compared to pH_{ini} was usually observed prior to the main sulfate reduction, which was most pronounced at low initial pH values (Fig. 1C). At the end of the incubation period all growing cultures reached a circum neutral pH, irrespective of the initial pH of the medium (Fig. 1C). The main sulfate reduction started after a certain lapse of time (designated as 'lag phase SR'), which generally lasted longer at more acidic pH conditions (Fig. 1D).

Average cell length and width for all samples retrieved at the end of incubation was 1.7±0.4 µm and 0.4±0.1 µm, respectively. Overall, the variation of cell width was of such low magnitude that it fell within the range of the resolving capacity of the microscope. Cell length appeared to be dependent on both growth phase and pH (Supporting information Fig. S1). As was expected, cells were significantly (Kruskal-Wallis; $p < 0.05$) longer in the early growth phase compared to the stationary phase. Furthermore, during the early growth phase, cells were significantly (Kruskal-Wallis; $p < 0.05$) longer in cultures at lower pH values compared to those at higher pH values. At pH 3.9 and pH 4.9 (which corresponded to the pH values during the early growth phase in the cultures at pH_{ini} 2.6 and pH_{ini} 4.5, respectively) average cell lengths were 2.4±0.6 µm and 2.5±0.7 µm, respectively. At pH 6.4 (pH_{ini} 6.3), the average cell length was only 1.7±0.4 µm.

Growth in the liquid phase and biofilm formation at pH_{ini} 3 as a function of time

In the culture liquid an increase in cell numbers was observed after 21 days (Fig. 2A). The exponential increase until day 38 corresponded to a division rate of 0.39 d^{-1} and a generation time of 62 h. A pronounced increase in pH and a pronounced decrease in sulfate, however, were only observed thereafter (Fig. 2B). A first visual change occurred at day 38 when the previously clear growth medium turned turbid with a fine whitish precipitate forming. A blackening of the culture liquid was only observed on day 49. This was also the time point when all Al and Fe had been removed from the aqueous phase (Fig. 2C). Overall, average cell length increased during the lag phase with a maximum of 3.1±0.8 µm and decreased during the exponential and early stationary phase reaching a minimum of 1.9±4 µm (Fig. 2D). Despite high variation in cell length differences were significant (Kruskal-Wallis; $p < 0.05$) between exponential/stationary phase and lag phase with the exception of day 21 (Supporting Information Fig. S2). The relatively short cell lengths and increased cell numbers in one of the duplicate samples at day 21 indicated that in this particular batch culture growth had started earlier. Average cell width for all samples was 0.5±0.1 µm and no pronounced changes depending on the growth phase were observed.

Biofilms grown on the two different solid substrata (glass and polycarbonate) did not reveal obvious differences in respect of cell density or biofilm 3-D structure as observed by CLSM (exemplarily shown for mature biofilms from day 57 in Supporting Information Fig. S3). Mainly single cells, more or less evenly spread, were observed on the substratum early on at day 28 (Fig. 3A – C). The signal for the nucleic acid stain corresponded to the signal for the protein stain. While the cells in the liquid culture had already reached early stationary phase at day 38, only a small increase in colonization of the substratum was found. The biofilm was

still organized to a great extent as a cell monolayer, though displaying an increasing number of microcolonies and associated particles. Particles at this stage were mostly seen in transmission mode and not in CLSM reflection mode indicating an amorphous structure (Supporting Information Fig. S4). In contrast, after 49 days, a relatively thick, patchy looking biofilm with mineral precipitates had developed (Fig. 3D – M). Below the gas-liquid interface microcolonies were identified which were more or less uniformly distributed (Fig. 3D – H). The protein signal still exhibited the contour of the cell, however, the signal of the nucleic stain was limited to a much narrower region, more central to the cell (Fig. 3E, F). Minerals with high reflection signal intensities were abundant in the upper region. In addition, larger mineral aggregates of different sizes and with overall lower reflection signal intensities were detected (Fig. 3I – M). The surfaces of these larger mineral aggregates were in parts densely covered with cells. The overall protein signal was weaker and also corresponded to the reflection signal (Fig. 3K, 3M). Biofilms did not change noticeably with respect to cell density and mineral precipitates after day 49 (for direct comparisons with biofilms sampled at day 63 see Supporting Information Fig. S5). Cell densities reached $139\pm58\cdot10^6$ and $71\pm44\cdot10^6$ cells cm^{-2} at the top and bottom side of the carrier, respectively. This would equal to $191\pm81\cdot10^6$ biofilm cells ml^{-1} and account for 91% of the total population in a 50-ml batch culture (with $18\pm2\cdot10^6$ planktonic cells ml^{-1} for the corresponding batches).

Investigation by SEM/EDX revealed two kinds of Al-rich precipitates at an early stage of biofilm formation (day 38) (for EDX spectra see Supporting Information S6). First, Al precipitates formed a thin and primarily smooth layer on the carrier surface (Fig. 4A). Cracks and scales were most likely artifacts resulting from dehydration during SEM sample preparation. Cells were exclusively found on top of this layer, suggesting that the layer formed prior to cell adhesion. Secondly, globules rich in Al and of different sizes were

formed and could be found partly embedded in the Al layer or on top of it, as individuals or in larger aggregates with cells attached to them (Fig. 4A, B). In the more mature biofilm (day 49), aggregates also contained precipitates with a 'flaky' appearance which were enriched in Fe and S next to Al (Fig. 4C; for EDX spectra see Supporting Information S7). The Fe:S ratio was 1.13±0.07 (mean ± standard deviation; n = 4). More cells were observed which were completely covered with Al-rich globules, some cells showed a damaged cell envelope (Fig. 4D). At the liquid-gas interface conspicuous crystals formed that were arranged as edges of a cross or a star (Fig. 4E, F). These minerals had a layered structure and gave very strong signals for both Fe and S (for EDX spectra see Supporting Information S8). The Fe:S ratio was 1.11±0.12 (mean ± standard deviation; n = 4). An average cell length of 2.41±0.24 and 2.29±0.24 µm and an average cell width of 276±34 and 330±32 nm were determined for day 38 and day 49, respectively. Whereas the difference in cell length was not significant it was significant in cell width (t-Test; $p < 0.05$).

Ultrathin sections in TEM revealed needle-like structures rich in Fe and S corresponding to cross-sections of flakes seen in SEM as well as circular structures rich in Al (Fig. 5A). Al-rich globules were directly attached to cell surfaces and seemed to 'sit' on the cells (Fig. 5B) whereas FeS minerals were randomly dispersed. No Al or FeS precipitates were found within the cells. TEM suggested a Gram-negative cell wall type showing a pronounced three-layer morphology consisting in general of the cytoplasmic membrane, a thin murein layer, and an outer membrane (Fig. 5B).

Phylogeny of strain 3baa

The 16S-rRNA gene of sulfate reducing strain 3baa (1442 nucleotides) exhibited 98% sequence similarity to the 16S rRNA gene of *T. narugense* Na82^T and *T. acidiphilum* 3127-1^T.

T. narugense Na82^T was isolated from pH-neutral hot spring Narugo in Miyagi, Japan (58°C, pH 6.9; Mori et al. 2003) and *T. acidiphilum* 3127-1^T was isolated from acidic thermal spring Oil site of the Uzon caldera, Kamchatka, Russia (60°C, pH 4.8; Frolov et al. 2017). Interestingly, strain 3baa forms a separate cluster with two sequences obtained from enrichments or directly from sediments of acidic Rio Tinto, Spain (HQ730662, JQ420033; Sanchez-Andrea et al. 2011, 2013) (Fig. 6). High sequence similarities (≥97%) were also shown to sequences retrieved from previous enrichments from sediments of mine pit lake 111 (Meier et al. 2012), and to environmental sequences found in microbial mats of Los Azufres geothermal field, Mexico (Brito et al. 2014) and thermal pool Arkashin of the Uzon caldera, Kamchatka, Russia (Burgess et al. 2012). According to current taxonomy in RDP-II the Thermodesulfobiaceae belong to the order of Thermoanaerobacterales within the class of Clostridia of the phylum Firmicutes. Other authors (Mori et al. 2003, Muyzer & Stams 2008, Kunisawa 2015) suggested a placement outside the Firmicutes.

Discussion

Acidophilic sulfate reducing bacteria and their pH range and optimum for growth

Based on 16S-rRNA gene sequence similarity, strain 3baa is more closely related to sequences obtained from other environments of moderate temperature than it is to the thermophilic species, *T. narugense* Na82^T and *T. acidiphilum* 3127-1^T, and hence might present a different species. Chemolithoautotrophic growth, cell morphology, a Gram-negative cell wall structure, and the lack of flagella and/or motility are common to all three strains. In contrast to strain Na82^T with a pH range of 4.0 – 6.5 and a pH optimum at pH 5.5 – 6.0 (Mori et al. 2003), and strain 3127-1^T with a pH range of 3.7 – 6.5 and a pH optimum at 4.8 – 5.0 (Frolov et al. 2017), strain 3baa showed a preference for more acidic conditions.

The pH range of growth expanded to pH 2.6 with highest amounts of sulfate reduced at pH ≤4.2. The pH ranges of growth determined for acidophilic *D. acidiphilus* SJ4^T and *D. acididurans* M1^T were pH 3.6 – 5.5 (optimum at pH 5.2) (Alazard et al. 2010) and pH 3.8 – 7.0 (optimum at pH 5.5) (Sánchez-Andrea et al. 2015).

However, direct comparisons of pH ranges and pH optima for growth are constrained by several factors. In this study the formation of Al hydroxides and Fe sulfides buffered in the lower pH range of growth. While in other studies phosphate (e.g. Mori et al. 2003, Frolov et al. 2017) or citrate buffers (e.g. Alazard et al. 2010) were used, these buffers appeared to be inhibitory to strain 3baa at low pH (unpublished results). A carbonate buffer (e.g. Sánchez-Andrea et al. 2015) is only effective in the circum neutral pH range. Electron donors will also have an impact on growth if these are weak organic acids (e.g. lactate, acetate) or if these are metabolized to acetate (e.g. glycerol, ethanol) (Rabus et al. 2013). Weak organic acids function as a proton transporter into the cell (Kimura et al. 2006, Slonczewski et al. 2009), leading to acidification of the cytoplasm and growth inhibition. This inhibitory effect does not occur when SRP are growing on H_2 and CO_2, and it may explain why chemolithoautotrophs tolerate lower pH values than chemoorganoheterotrophs.

In order to determine the pH range and pH optimum for growth of SRPs, sulfate reduction rates are often determined (e.g. Mori et al. 2003, Alazard et al. 2010, Sánchez-Andrea et al. 2015). However, high SRRs do not necessarily relate to high growth rates and/or high growth yields (e.g. Knoblauch & Jørgensen 1999). The high SRRs could have resulted from high respiration rates in order to remove protons from the cytoplasm by means of primary proton pumps. Along with the down-regulation of the F_1F_0-ATPase to limit the influx of protons this represents a common mechanism for pH homeostasis displayed by acidophiles and neutrophiles alike under low pH conditions (Slonczewski et al. 2009, Krulwich et al. 2011,

Mols & Abee 2011). Both, low ATP synthesis and the relocation of energy towards cell maintenance instead of cell growth, would result in a lower growth yield. Although cell numbers were low in the culture liquid at low pH conditions, the majority of the biomass was located in the biofilm. We therefore assume that high SRRs were linked to energy generation (ATP synthesis) and biosynthesis in strain 3baa, even at lower pH values. Microniches with higher pH values may have been present within the biofilm (see discussion below), nonetheless most cells appeared to sit on top of the minerals being directly exposed to the culture liquid. Strain 3baa needed much longer to adapt under more acidic pH conditions. In addition, elongated cells or filamentation is a common response of bacteria to environmental stresses including acid stress (Krüger et al. 1994, Everis & Betts 2001, Justice et al. 2008). It may result from disturbance and malfunctioning of cell components involved in cell division. At low pH (≤3.5) the protein FtsZ will not assemble to protofilaments required for cell division (Santra & Panda 2007). This would imply at least a transient acidic intracellular pH. Further investigations are needed in order to find out how strain 3baa adapts to acidic conditions and what mechanisms of pH homeostasis it deploys in planktonic and sessile state.

Biofilm formation and the role minerals may play in it

Biofilm growth may also present a defense mechanism against unsuitable environmental conditions (Slonczewski et al. 2009, Lemire et al. 2013, Flemming et al. 2016). Within the biofilm matrix (which is most often organic), the transport of solutes is generally diffusion controlled. If protons are consumed faster by sulfate reduction than the rate of diffusion, microniches with higher pH levels may form. Using a simple diffusion-based model proposed by Koschorreck (2008) and estimates for cellular sulfate reduction rates (cSRR), we

calculated the minimum biofilm thickness needed to sustain an internal pH 4 at an external pH 3 (for calculation see Supporting Information S2). At a rate of 6.89 fmol SO_4^{2-} $cell^{-1}$ d^{-1}, the minimum thickness was estimated to be 250 µm which was well above the observed maximum height of 100 µm. However, under the assumption that cSRR were probably higher during early biofilm formation and that proton diffusion rates were possibly lower within the biofilm, slightly elevated pH values in the centre of larger microcolonies could not be ruled out completely. Different sulfate reducers including members of the genera *Desulfovibrio*, *Desulfobacterium*, and *Desulfomicrobium* were shown to produce copious amounts of EPS which consist of various amounts of polysaccharides, proteins and/or DNA (Zinkevich et al. 1999, Chan et al. 2002, Hockin & Gadd 2003, Beech & Sunner 2004, Braissant et al. 2007, Yang et al. 2016). The production of an extensive polysaccharide matrix is not necessarily a prerequisite for the adhesion to solid surfaces and biofilm formation as was shown for *Desulfovibrio vulgaris*, which used flagella to establish and maintain biofilm structure (Clark et al. 2007). In the case of strain 3baa, neither the production of EPS matrix nor protein filaments was observed. Biofilm formation was apparently linked to the precipitation of Al hydroxides and Fe sulfides.

Although the globular Al-rich precipitates obtained here were almost identical in appearance and size to Al hydroxysulfates found in anoxic waters of acidic pit lakes (Sánchez-España et al. 2016a), we could not detect sulfur by EDX. This suggests the formation of Al hydroxides in our cultures instead of Al hydroxysulfates. The formation of X-ray-amorphous $Al(OH)_3$ and microcrystalline gibbsite was observed for acidic effluents enriched in Al mixing with near neutral surface water in the pH range 4.2 – 4.9 (Furrer et al. 2002). Aluminum started to precipitate in our cultures at pH 3.5 – 3.7. If Al precipitation had only taken place on bacterial cell surfaces in the culture liquid, more cells covered with Al precipitates should

have already been observed at the early stage of biofilm formation. On the contrary, most cells detected were free of Al precipitates. The cell wall charge of Gram-negative and Gram-positive bacteria is considered to be very similar despite large differences in macromolecular structures (Claessens et al. 2006). The most prominent proton and metal binding sites at the bacterial surface are carboxyl functional groups with low p*Ka* (4 – 5) values, phosphate functional groups with neutral p*Ka* (6 – 7) values, and hydroxyl as well as amine functional groups with high p*Ka* (8 – 9) values (Fein et al. 1997, Cox et al. 1999, Haas 2004). Although the exact composition of the outer membrane of strain 3baa is not known, the presence of lipopolysaccharides rich in phosphate and carboxyl functional groups may be postulated (Fortin & Beveridge 2000). At low pH (<4) all phosphate sites and the majority of carboxyl sites would be protonated and bacterial surfaces would have a low affinity for Al cations. With increasing pH, the sites become deprotonated allowing the binding of Al cations, heterogeneous nucleation, and subsequently mineral precipitation. This may explain why the majority of cells were covered with Al-rich spheres in the more mature biofilm. Interestingly, the bacterial cells only colonized the carrier surface after an amorphous Al hydroxide layer had formed. This suggested that an increased affinity for Al-hydroxides probably enabled biofilm formation. The average value of the point of zero charge (PZC) for amorphous Al hydroxide and gibbsite is 9.0 (Karamalidis & Dzombak 2010). At pH below the PZC, the net surface charge of the mineral is positive and this would enhance the ionic interaction with the negative net surface charge of the bacterium. Here, the Al hydroxides, instead of polysaccharides or proteins, appear to be functioning as 'glue', cementing the cells to the solid surface and holding microcolonies, i.e. the growing biofilm, in place. Unlike Al precipitates, FeS precipitates were not encountered directly on cell surfaces in our cultures. In contrast to Al^{3+} as well as Fe^{3+}, Fe^{2+} shows a low affinity towards carboxyl or

phosphate groups even at near neutral pH (Lemire et al. 2013). Instead, Fe^{2+} interacts more strongly with other functional groups, such as sulfhydryl, imidazole, and phenyl groups, all of which are rarely displayed at the cell surface. Sulfhydryl groups account for only 5 – 10% of the total binding sites on the cell surface and have a relatively high p*Ka* value of ~7 (Nell & Fein 2017). This may explain why the precipitation of FeS is only minor at least on intact cells. Mackinawite and also greigite appear to form as main mineral products in biotically mediated as well as purely chemical precipitation of iron sulfides from aqueous sulfide and aqueous ferrous iron (e.g. Herbert et al. 1998, Ohfuji & Rickard 2006, Gramp et al. 2010, Csákberényi-Malasics et al. 2012, Picard et al. 2018). Nanoparticulate mackinawite is usually the first condensed phase precipitating and its composition closely approximates stoichiometric FeS (Rickard & Morse 2005). Despite the Fe:S ratio of >1, based on the precipitate morphology (the platy structure of Fe and S rich 'flakes' as well as the layered structure of crystals arranged as crosses or stars), we presume that mackinawite also formed in our cultures. Mackinawite possesses a layer structure where the Fe atoms form sheets and the tetrahedrally coordinated S atoms to both sides shield the Fe sheets (Wolthers et al. 2003). The FeS crystal grows in a tabular form with the most prominent surface being apolar and the least reactive (Wolthers et al. 2005, Dzade et al. 2014). This may lessen the affinity of the negatively charged bacterial cells. Still, we observed a densely populated carrier surface with pronounced microcolony formation consisting of both minerals and bacterial cells.

Conclusions

Thermodesulfobium sp. strain 3baa is considered to be acidophilic, however, the exact degree of its acidophily is still to be determined. The attachment to solid surfaces enables

strain 3baa to attain high sulfate reduction and growth rates, even at lower pH levels. Mineral precipitation may play a crucial role in biofilm formation as illustrated in Figure 7. Sulfate reduction by planktonic cells proceeds at very low rates at pH ≥2.5 (Fig. 7A), leading to a slight increase of pH, and the precipitation of Al hydroxides at pH ≥3.5 (Fig. 7B). Al hydroxides and bacterial cells most likely interact based on electrostatic attraction of oppositely charged surfaces, permitting the attachment of cells to solid surfaces and the growth of microcolonies (Fig. 7C). Increasing cell numbers and higher sulfate reduction rates eventually lead to the precipitation of Fe sulfides at pH ≥4.5 (Fig. 7D). Mineral precipitation does not seem to hamper further growth. On the contrary, mineral surfaces appear to provide a favorable microenvironment for growth. In a natural setting, such as the sediments of acidic mine pit lake 111, growth may occur on clay minerals and quartz minerals coated with Al/Fe hydroxides/hydroxysulfates. In engineered systems, the achievement of stable biofilms and high sulfate reduction rates are of particular importance for an effective treatment of acidic metal-rich waste waters. Hence, further investigations should address in more detail cell-mineral interactions and the possible effects on the physiological state of cells at low pH conditions.

Material and Methods

Source and isolation of bacterial strain 3baa

The sulfate reducing strain 3baa was isolated from sediments of acidic mine pit lake 111 situated in the Lusatian lignite mining district in Brandenburg, Germany (Büttner et al., 1998; Meier et al., 2004). A sediment core was retrieved from the northern basin at a water depth of 6 m. At this site, the water temperature above the sediments varies annually from 2 – 11°C. Oxygen may penetrate into the sediments to a maximum depth of 10 mm. During lake

stratification, the sediments can also become completely anoxic. The pH in the top 10 cm of sediments ranges from 2.6 to 3.0 with a slight increase with depth. The main pore water ions are calcium (4.8 – 5.9 mM), magnesium (1.1 – 1.3 mM), iron (0.7 – 7.9 mM), aluminum (1.1 – 1.7 mM), and sulfate (9 – 16 mM) (Herzsprung et al., 2002). Sediment from the depth interval of 1 – 5 cm was taken as inoculum for the primary enrichment culture.

The composition of the mineral medium used for enrichment and subsequent isolation was adapted to pore water ion concentrations and contained per liter 0.5 mM Na_2SO_4, 1 mM KCl, 1 mM $MgSO_4 \cdot 7H_2O$, 6 mM $CaSO_4 \cdot 2H_2O$, 2 mM $Al_2(SO_4)_3 \cdot 18H_2O$, 5 mM $FeSO_4 \cdot 7H_2O$, 0.5 mM $Na_2SiO_3 \cdot 9H_2O$, 0.05 mM $MnSO_4 \cdot H_2O$, 0.02 mM $ZnCl_2$, 2 mM NH_4Cl, and 1 mM KH_2PO_4 (Meier et al. 2012). According to Widdel & Bak (1992), 1 ml vitamin solution, 1 ml non-chelated trace element solution and 100 µl selenate-tungstate solution were added per liter of medium. The pH of this artificial pore water medium (APWM) was set to pH 3 using 0.5 M H_2SO_4. Sulfate reducers were grown with H_2 as electron donor and CO_2 as carbon source. Accordingly, headspaces of serum bottles as well as anaerobic jars were purged with 80% H_2/20% CO_2. Cultivation in liquid media was conducted in 125-ml serum bottles containing 50 ml APWM. Isolation was performed by a modified roll-tube technique (Widdel & Bak 1992) using 50-ml centrifuge tubes incubated in anaerobic jars with catalyst (HP0011A, Oxoid, Basingstoke, UK). Gellan gum (GELRITE™, Roth, Karlsruhe, Germany) served as gelling agent at a final concentration of 0.6%. After several weeks to months colonies became visible. Single colonies were picked and transferred to liquid medium. The isolation procedure was repeated at least two times. All incubations took place in the dark at 25°C. Incubations at temperatures closer to ambient values (15 and 20°C) had led eventually to the enrichment of representatives of the same species (unpublished results). Medium preparation, isolation procedures, and sampling were carried out within an anaerobic

chamber using a 95% N_2/5% H_2 gas mixture and a palladium catalyst (Vinyl Anaerobic Airlock Chamber, Coy Laboratory Products Inc., Grass Lake, MI). The culture was checked for chemoorganoheterotrophic contaminants (for details see Supporting Information S1).

Growth experiments

Growth experiments were performed as batch cultures in 125-ml serum bottles containing APWM and H_2/CO_2 in the headspace as described above. The bottles were inoculated with 1 vol% culture of strain 3baa pre-grown in liquid APWM set to pH 3 and incubated on a horizontal shaker set to 200 rpm at 25°C in the dark over a time period of approximately 60 days. In order to determine the pH optimum for growth, a batch series was conducted with APWM set to eleven different initial pH values (pH_{ini}) in the range of pH 2 – 7 at intervals of approximately 0.5 pH units. For each of the eleven values of pH_{ini}, growth experiments were performed in duplicate, with the exception of pH_{ini} 2.5 and 3.0 for which growth experiments were performed in two series with two replicates in the first and one replicate in the second. The bottles were sampled every 3 to 5 days and the culture liquid was analysed for pH and sulfate. Cell numbers and sizes were determined at the end of incubation (stationary growth phase) and for the cultures at pH_{ini} 2.6, 4.5, and 6.3 also during the early growth phase (just before the main sulfate reduction phase started). In order to investigate biofilm formation by strain 3baa, a batch series was performed with a total of twenty bottles. Each contained APWM pH_{ini} 3.2 and one removable carrier (11.5 x 76 mm) made of either polycarbonate (PC) or glass (G). The carriers stood almost upright and were submersed for the lower 3.8 cm. For each sampling every 6 to 11 days, two bottles, one with PC and one with G carrier, were sacrificed, with the exception of day 28 when a total of four bottles was sampled. The carriers were removed, rinsed with sterile 0.9% NaCl and stored under anoxic conditions in

0.9% NaCl with 4% formaldehyde for CLSM (G) or Karnovsky fixative (Karnovsky 1965) for EM (PC). The liquid phase was sampled for the determination of pH, cell number and size, sulfate, and the dissolved elements Al and Fe. To estimate biofilm cell numbers, two additional bottles with G carriers were incubated. At the end of incubation, the biofilm was scraped off with a razorblade and collected in 1 ml 0.9% NaCl. The area available for colonization included the submersed surface of the carrier (2x 4.4 cm^2) as well as the submersed side walls (43.7 cm^2) and the bottom (18.1 cm^2) of the bottle when filled with 50 ml medium.

Analytical methods

Measurement of pH was performed directly upon sampling using a SenTix 940 pH electrode and a Multi 3430 SET F meter (WTW, Weilheim, Germany). Dissolved Al, Fe, and Mg were determined by atomic absorption spectroscopy (AAnalyst 400, Perkin Elmer, Waltham, USA). Samples were 0.2-µm filtered and acidified with HNO_3 (2%). For sulfate measurements either 0.2-µm filtered samples or the supernatant after centrifugation at 16,000 x *g* for 15 min were used. Sulfate was determined by ion chromatography using an IC 690 (Metrohm, Herisau, Switzerland) equipped with a PRP-X100 column (Hamilton, Bonaduz, Switzerland) and 2 mM Na-benzoate as eluent. Sulfate measurements were performed on one sample (batch series to determine pH optimum for growth) or triplicate samples (batch series to investigate biofilm formation).

Cell counts and cell measurements

Samples were fixed with formaldehyde (4%) and stored under anoxic conditions. Aliquots of cell suspensions were treated with 10% methanol (or 4% NaCl for biofilm samples),

ultrasonication and 0.5 M HCl prior to filtering on black membrane filters of 0.2-µm pore size (Isopore GTBE; Merck Millipore, Darmstadt, Germany) and staining with 1:250 diluted nucleic acid stain SYBR Green I (Molecular Probes, Eugene, Oregon, USA). Per sample one (batch series to investigate biofilm formation) or two filters (batch series to determine pH optimum for growth; biofilm samples) were prepared and 30 images per filter were recorded using AxioImager.M2 epifluorescence microscope (Carl Zeiss Microscopy, Jena, Germany) and a 38HE filter set. Width and length measurements were performed on approximately 30 cells per filter.

Confocal laser scanning microscopy (CLSM)

Staining and microscopic examination followed immediately after removing the respective carrier from the anoxic storing device. Carriers were rinsed with ultrapure water and stained with 1:1000 diluted nucleic acid stain SYBR Green I and 1:1000 diluted protein stain SYPRO Red (Molecular Probes, Eugene, Oregon, USA). Subsequently carriers were placed in Petri dishes and submersed in water. Samples were examined with an upright TCS SP5X confocal laser scanning microscope (Leica Microsystems, Wetzlar, Germany) equipped with a supercontinuum light source. Imaging was done with the two long distance, water immersible lenses 25x NA 0.95 and 63x NA 0.9. For orientation, the carrier was divided into 1 cm segments, whereby the lower end corresponded to 0 – 1 cm and the upper end, above the liquid-gas interface, to 4 – 5 cm. Signals were recorded in i) the green channel for SYBR Green I (excitation, 490 nm; emission, 510 to 580 nm), ii) the red channel for SYPRO Red (excitation, 550 nm; emission, 600 to 700 nm), and iii) the grey channel for the CLSM-reflection mode (excitation, 490 nm; emission, 485 to 495 nm). Stepsize for sections was 0.5 µm. Imaging was performed using the microscope software LASAF version 2.6.1 (Leica

Microsystems, Wetzlar, Germany). Data sets were further processed using the software IMARIS versions 8.3.1 (Bitplane, Zurich, Switzerland).

Electron microscopy and micro-analysis

For electron microscopy PC carriers were cut into 1-cm segments corresponding to the scheme applied for CLSM. In order to minimize the exposure of wet samples to oxygen, all steps including fixation, segmentation, rinsing, and in case of SEM also the ethanol series were carried out in the anaerobic chamber. After retrieval from the Karnovsky fixative, carrier segments were rinsed 3x in 0.1 M cacodylate buffer. For scanning electron microscopy (SEM), samples were subsequently dehydrated in a graded ethanol series and a final replacement of the ethanol by hexamethyldisilazane. Samples were coated with 20 nm Au. For transmission electron microscopy (TEM), samples were postfixed with 1% OsO_4 . Samples were then dehydrated, treated with propylene oxide and embedded in Spurr resin (Sigma-Aldrich, Munich, Germany). Ultra-thin sections of 70 nm were placed on copper grids and contrasted with uranyl acetate (2% in H_2O) and lead citrate (3%, pH 12; Ultrostain 2, Laurylab, Brindas, France). Samples ready for microscopic investigation were stored under vacuum. Samples were viewed in a SEM Zeiss Gemini 1530 and a TEM Zeiss EM910, both equipped with an INCA EDX detector (Oxford Instruments, Abingdon, UK) for energy-dispersive X-ray micro-analysis. Length and width of 25 cells were determined from SEM images of selected samples.

16S rRNA gene analysis

Cells for DNA extraction were obtained from 10 ml stationary phase liquid culture by centrifugation at 4,200 x *g* and 10°C for 15 min and pellets washed two times in TE buffer (10

mM TRIS-HCl, 1 mM EDTA; pH 8). Genomic DNA was extracted using the PowerSoil® DNA Isolation Kit from MoBio Laboratories Inc. (Sued-Laborbedarf, Gauting, Germany). Bacterial 16S rRNA genes were amplified from DNA extracts using the universal bacterial primers 27f and 1492r (Biomers, Ulm, Germany; for sequences see supporting material Table S1). Amplification was performed by an initial denaturation step at 94°C for 4 min, 30 cycles of 45 s at 94°C, 1 min at 58°C, and 2 min at 72°C, followed by a final extension step at 72°C for 10 min. PCR products were purified with the Isolate PCR and Gel Kit (Bioline, Luckenwalde, Germany). Sequencing of forward and reverse strand was performed by LGC Genomics (Berlin, Germany). The partial sequences were manually checked for ambiguous sequences and assembled applying the Manual Sequence Alignment Editor version 11/2001 (SequentiX, Klein Raden, Germany). The BLASTN program (www.ncbi.nlm.nih.gov/BLAST; Zhang et al. 2000, Morgulis et al. 2008) was used to search for similar sequences in the GenBank nucleotide sequence database, and the Sequence Match tool was used to search for similar sequences compiled by the Ribosomal Database Project-II Release 11.3 (http://rdp.cme.msu.edu; Cole et al. 2014). The determined 16S rRNA gene sequence has been deposited in the GenBank nucleotide sequence database under accession no. KY928402. Sequences selected for phylogenetic tree construction were retrieved from RDP and NCBI and aligned using ClustalX 2.1 (http://www.clustal.org/clustal2; Larkin et al. 2007) choosing the default settings for accurate pairwise comparison and the option to iterate each alignment step. The alignment was checked using the Manual Sequence Alignment Editor version 11/2001 and short or poorly aligned sequences were removed. The remaining sequences were trimmed to the same length so that the alignment still covered 1390 bp. Trees were constructed again in ClustalX 2.1 using the Neighbour Joining algorithm and 1000

bootstrap trials and drawn with NJplot (http://doua.prabi.fr/software/njplot; Perrière & Gouy 1996).

Determination of sulfate removal rates and statistical analysis

Sulfate removal rates (SRR) were determined as the coefficient of linear regression for the time interval showing a distinct maximum linear decrease of sulfate concentration. As the time interval matched for duplicate batches, data sets were combined for linear regression analysis performed with Microsoft Office Excel 2007. Standard errors (S.E.) of coefficients were determined. Statistical analysis of cell numbers, cell length, and cell width (the latter only from those measurements obtained from SEM images) was performed using IBM SPSS Statistics 23 (IBM, Ehningen, Germany). Normal distribution was checked using the tests of Kolmogorov-Smirnov ($n \geq 50$) or Shapiro-Wilk ($n < 50$). When the data for mean comparison was normally distributed a t-test or one factorial ANOVA was performed using post hoc analysis of Bonferroni (in case of homogeneity of variances) or Dunnett-T3 (in case of non-homogeneous variances). For non-normally distributed data a comparison according to Kruskal-Wallis was performed.

Acknowledgements

Brigitte Mann and Ulli Bange at the University of Koblenz-Landau, Institute for Integrated Natural Sciences, are thanked for atomic absorption spectroscopy and ion chromatography analysis. Ute Kuhlicke from the Helmholtz Centre of Environmental Research, Department of River Ecology, is acknowledged for her support with confocal laser scanning microscopy and image analysis. Silke Loch and Liane Junglas from the Federal Armed Forces Central Hospital

Coblenz are thanked for assistance with electron microscopy. All authors declare no conflict of interest.

References

Alazard, D., Joseph, M., Battaglia-Brunet, F., Cayol, J.-L., and Ollivier, B. (2010) *Desulfosporosinus acidiphilus* sp. nov.: a moderately acidophilic sulfate-reducing bacterium isolated from acid mining drainage sediments. Extremophiles 14: 305-312.

Barton, L. L., and Fauque, G. D. (2009) Biochemistry, physiology and biotechnology of sulfate reducing bacteria. Adv Appl Microbiol 68: 41-98.

Beech, I. B., and Sunner, J. (2004) Biocorrosion: towards understanding interactions between biofilms and metals. Curr Opin Biotechnol 15: 181-186.

Bijmans, M. F. M., De Vries, E., Yang, C.-H., Buisman, C. J. N., Lens, P. N. L. , and Dopson, M. (2010) Sulfate reduction at pH 4.0 for treatment of process and wastewaters. Biotechnol Prog 26: 1029-1037.

Blowes, D. W., Ptacek, C. J., Jambor, J. L., and Weisener, C. G. (2003) The geochemistry of acid mine drainage. Treatise Geochem 9: 149-204.

Bradley, A. S., Leavitt, W. D., and Johnston, D. T. (2011) Revisiting the dissimilatory sulfate reduction pathway. Geobiology 9: 446-457.

Braissant, O., Decho, A. W., Dupraz, C., Glunk, C., Przekop, K. M., and Visscher, P. T. (2007) Exopolymeric substances of sulfate-reducing bacteria: Interactions with calcium at alkaline pH and implication for formation of carbonate minerals. Geobiology 5: 401-411.

Brito, E. S., Villegas-Negrete, N., Sotelo-González, I., Caretta, C., Goñi-Urriza, M. Gassie, C., et al. (2014) Microbial diversity in Los Azufres geothermal field (Michoacán, Mexico) and isolation of representative sulfate and sulfur reducers. Extremophiles 18: 385-398.

Burgess, E., Unrine, J., Mills, G., Romanek, C., and Wiegel, J. (2012) Comparative geochemical and microbiological characterization of two thermal pools in the Uzon Caldera, Kamchatka, Russia. Microb Ecol 63: 471-489.

Büttner, O., Becker, A., Kellner, S., Kuehn, B., Wendt-Potthoff, K., Zachmann, D. W., and Friese, K. (1998) Geostatistical analysis of surface sediments in an acidic mining lake. Water Air Soil Pollut 108: 297-316.

Chan, K.-Y., Xu, L.-C., and Fang, H.H.P. (2002) Anaerobic electrochemical corrosion of mild steel in the presence of extracellular polymeric substances produced by a culture enriched in sulfate-reducing bacteria. Environ Sci Technol 36: 1720-1727.

Chen, L., Huang, L., Méndez-Garcia, C., Kuang, J., Hua, Z., and Shu, W. (2016) Microbial communities, processes and functions in acid mine drainage ecosystems. Curr Opin Biotechnol 38: 150-158.

Claessens, J., Van Lith, Y., Laverman, A.M., and Van Cappellen, P. (2006) Acid-base activity of live bacteria: Implications for quantifying cell wall charge. Geochim Cosmochim Acta 70: 267-276.

Clark, M.E., Edelmann, R.E., Duley, M.L., Wall, J.D., and Fields, M.W. (2007) Biofilm formation in *Desulfovibrio vulgaris* Hildenborough is dependent upon protein filaments. Environ Microbiol 9: 2844-2854.

Cole, J.R., Wang, Q., Fish, J.A., Chai, B., McGarrell, D.M., Farris, R. J., et al., (2014) Ribosomal Database Project: data and tools for high throughput rRNA analysis. Nucleic Acids Res 42: D633-D642.

Cox, J.S., Smith, D.S., Warren, L.A., and Ferris, F.G. (1999) Characterizing heterogeneous bacterial surface functional groups using discrete affinity spectra for proton binding. Environ Sci Technol 33: 4514-4521.

Csákberényi-Malasics, D., Rodriguez-Blanco, J.D., Kis, V.K., Rečnik, A., Benning, L.G., and Pósfai, M. (2012) Structural properties and transformations of precipitated FeS. Chem Geol 294–295: 249-258.

Donald, R., and Southam, G. (1999) Low temperature anaerobic bacterial diagenesis of ferrous monosulfide to pyrite. Geochim Cosmochim Acta 63: 2019-2023.

Dzade, N.Y., Roldan, A., and De Leeuw, N.H. (2014) The surface chemistry of NO_x on mackinawite (FeS) surfaces: a DFT-D2 study. Phys Chem Chem Phys 16: 15444-15456.

Everis, L., and Betts, G. (2001) pH stress can cause cell elongation in *Bacillus* and *Clostridium* species: a research note. Food Control 12: 53-56.

Falagán, C., Yusta, I., Sánchez-España, J., and Johnson, D.B. (2017) Biologically-induced precipitation of aluminium in synthetic acid mine water. Miner Eng 106: 79 – 85.

Fein, J.B., Daughney, C.J., Yee, N., and Davis, T.A. (1997) A chemical equilibrium model for metal adsorption onto bacterial surfaces. Geochim Cosmochim Acta 16: 3319-3328.

Flemming, H.-C., Wingender, J., Szewzyk, U., Steinberg, P., Rice, S.A., and Kjelleberg, S. (2016) Biofilms: an emergent form of bacterial life. Nat Rev Microbiol 14: 563-575.

Fortin, D., and Beveridge, T.J. (2000) Mechanistic routes to biomineral surface development. In Biomineralization: From Biology to Biotechnology and Medical Application. Baeuerlein, E. (ed.). Weinheim: Wiley-VCH, pp. 7-24.

Fortin, D., Southam, G., and Beveridge, T.J. (1994) Nickel sulfide, iron-nickel sulfide and iron sulfide precipitation by a newly isolated *Desulfotomaculum* species and its relation to nickel resistance FEMS Microbiol Ecol 14: 121-132.

Frolov, E.N., Kublanov, I.V., Toshchakov, S.V., Samarov, N.I., Novikov, A.A. Lebedinsky, A.V. et al. (2017) *Thermodesulfobium acidiphilum* sp. nov., a new thermoacidophilic sulfate-reducing chemoautotrophic bacterium from a Kamchatkan thermal site. Int J Syst Evol Microbiol 67: 1482-1485.

Furrer, G., Phillips, B.L., Ullrich, K.-U., Pöthing, R., and Casey, W.H. (2002) The origin of aluminum flocs in polluted streams. Science 297: 2245-2247.

Gallagher, K. L., Kading, T. J., Braissant, O., Dupraz, C., and Visscher, P. T. (2012) Inside the alkalinity engine: the role of electron donors in the organomineralization potential of sulfate-reducing bacteria. Geobiology 10: 518-530.

Geller, W., Schultze, M., Kleinmann, B., and Wolkersdorfer, C. (2013) Acidic Pit Lakes – The Legacy of Coal and Metal Surface Mines. Heidelberg: Springer.

Gramp, J.P., Bigham, J.M., Jones, F.S., and Tuovinen, O.H., (2010) Formation of Fe-sulfides in cultures of sulfate-reducing bacteria. J Hazard Mater 175: 1062-1067.

Haas, J. (2004) Effects of cultivation conditions on acid-base titration properties of *Shewanella putrefaciens* Chem Geol 209: 67-81.

Hard, B.C., Walther, C., and Babel, W. (1999) Sorption of aluminum by sulfate-reducing bacteria isolated from uranium mine tailings. Geomicrobiology J 16:4: 267-275.

Harrison, J.J., Ceri, H., and Turner, R.J. (2007) Multimetal resistance and tolerance in microbial biofilms. Nat Rev Microbiol 5: 928- 938.

Herbert, R.A., Benner, S.G., Pratt, A.R., and Blowes, D.W. (1998) Surface chemistry and morphology of poorly crystalline iron sulfides precipitated in media containing sulfate-reducing bacteria. Chem Geol 144: 87-97.

Herzsprung, P., Friese, K., Frömmichen, R., Göttlicher, J., Koschorreck, M., Tümpling Jr, W.V., and Wendt-Potthoff, K.(2002) Chemical changes in sediment pore-waters of an acidic mining lake after addition of organic substrate and lime for stimulating lake remediation. Water Air Soil Pollut: Focus 2: 123-140.

Hockin, S.L., and Gadd, G.M. (2003) Linked redox precipitation of sulfur and selenium under anaerobic conditions by sulfate-reducing bacterial biofilms. Appl Environ Microbiol 69: 7063-7072.

Justice, S.S., Hunstad, D.A., Cegelski, L., and Hultgren, S.J. (2008) Morphological plasticity as a bacterial survival strategy. Nat Rev Microbiol 6: 162-168.

Karnachuk, O.V., Mardanov, A., Avakyan, M.R., Kadnikov, V.V., Vlasova, M., Beletsky, A. V., et al. (2015a) Draft genome sequence of the first acid-tolerant sulfate-reducing deltaproteobacterium *Desulfovibrio* sp. TomC having potential for minewater treatment. FEMS Microbiol Lett 362: 1-3.

Karnachuk, O.V., Kurganskaya, I.A., Avakyan, M.R., Frank, Y. A., Ikkert, O.P., Filenko, R.A., et al. (2015b) An acidophilic *Desulfosporosinus* isolated from the oxidized mining wastes in the Transbaikal area. Microbiology (Transl. Mikrobiologiya) 84: 677-686.

Karamalidis, A.K., and Dzombak, D.A. (2010) Surface Complexation Modelling – Gibbsite, 1st edn. Hoboken NJ, USA: John Wiley & Sons.

Karnovsky, M.J. (1965), A formaldehyde-glutaraldehyde fixative of high osmolarity for use in electron microscopy. J Cell Biol 27: 137A-138A.

Kimura, S., Hallberg, K.B., and Johnson, D.B. (2006) Sulfidogenesis in low pH (3.8-4.2) media by a mixed population of acidophilic bacteria. Biodegradation 17: 159-167.

Knoblauch, C., and Joergensen, B.B. (1999) Effect of temperature on sulphate reduction, growth rate and growth yield in five psychrophilic sulphate-reducing bacteria from Arctic sediments. Environ Microbiol 1: 457-467.

Koschorreck, M. (2008) Microbial sulphate reduction at a low pH. FEMS Microbiol Ecol 64: 329-342.

Koschorreck, M., Geller, W., Neu, T., Kleinsteuber, S., Kunze, T., Trosiener, A., and Wendt-Potthoff, K. (2010) Structure and function of the microbial community in an in situ reactor to treat an acidic mine pit lake. FEMS Microbiol Ecol 73: 385-395.

Krüger, E., Völker, U., and Hecker, M. (1994) Stress induction of clpC in *Bacillus subtilis* and its involvement in stress tolerance. J Bacteriol 176: 3360-3367.

Krulwich, T.A., Sachs, G., and Padan, E. (2011) Molecular aspects of bacterial pH sensing and homeostasis. Nat Rev Microbiol 9: 330-343.

Kunisawa, T. (2015) Evolutionary relationships of completely sequenced Clostridia species and close relatives. Int J Syst Evol Microbiol 65: 4276-4283.

Küsel, K., Roth, U., Trinkwalter, T., and Pfeiffer, S. (2001) Effect of pH on the anaerobic microbial cycling of sulfur in mining-impacted freshwater lake sediments. Environ Exp Bot 46: 213-223.

Larkin, M.A., Blackshields, G., Brown, N.P., Chenna, R., McGettigan, P.A., McWilliam, H. Valentin, F., et al. (2007) Clustal W and Clustal X version 2.0. Bioinformatics 23: 2947-2948.

Lemire, J.A., Harrison, J.J., and Turner, R.J. (2013) Antimicrobial activity of metals: mechanisms, molecular targets and applications. Nat Rev Microbiol 11: 371–384.

MacLean, L.C.W., Tyliszczak, T., Gilbert, P.U.P.A., Zhou, D., Pray, T. J., Onstott, T.C., and Southam, G. (2008) A high-resolution chemical and structural study of framboidal pyrite formed within a low-temperature bacterial biofilm. Geobiology 6: 471-480.

Meier, J., Babenzien, H.D., and Wendt-Potthoff, K. (2004) Microbial cycling of iron and sulfur in sediments of acidic and pH-neutral mining lakes in Lusatia (Brandenburg, Germany). Biogeochemistry 67: 135-156.

Meier, J., Piva, A., and Fortin, D. (2012) Enrichment of sulfate-reducing bacteria and resulting mineral formation in media mimicking pore water metal ion concentrations and pH conditions of acidic pit lakes. FEMS Microbiol Ecol 79: 69-84.

Mols, M., and Abee, T. (2011) *Bacillus cereus* responses to acid stress. Environ Microbiol 13: 2835-2843.

Moreau, J.W., Weber, P.K., Martin, M.C., Gilbert, B., Hutcheon, I.D., and Banfield, J.F. (2007) Extracellular proteins limit the dispersal of biogenic nanoparticles. Science 316: 1600-1603.

Morgulis, A., Coulouris, G., Raytselis, Y., Madden, T.L., Agarwala, R., and Schäffer, A. A. (2008) Database indexing for production MegaBLAST searches. Bioinformatics 24: 1757-1764.

Mori, K., Kim, H., Kakegawa, T., and Hanada, S. (2003) A novel lineage of sulfate-reducing microorganisms: *Thermodesulfobiaceae* fam. nov., *Thermodesulfobium narugense*, gen. nov., sp. nov., a new thermophilic isolate from a hot spring. Extremophiles 7: 283-290.

Muyzer, G., and Stams, A.J.M. (2008) The ecology and biotechnology of sulphate-reducing bacteria. Nat Rev Microbiol 6: 441-454.

Ňancucheo, I., and Johnson, D.B. (2014) Removal of sulfate from extremely acidic mine waters using low pH sulfidogenic bioreactors. Hydrometallurgy 150: 222-226.

Nell, R.M., and Fein, J.B. (2017) Influence of sulfhydryl sites on metal binding by bacteria. Geochim Cosmochim Acta 199: 210-221.

Nordstrom, D.K. (2011) Mine waters: acidic to circumneutral. Elements 7: 393-398.

Ohfuji, H., and Rickard, D. (2006) High resolution transmission electron microscopic study of synthetic nanocrystalline mackinawite. Earth Planet Sci Lett 241: 227-233.

Peiffer, S. (2016) Reaction time scales for sulphate reduction in sediments of acidic pit lakes and its relation to in-lake acidity neutralisation. Appl Geochem 73: 8-12.

Perrière, G., and Gouy, M. (1996) WWW-Query: An on-line retrieval system for biological sequence banks. Biochimie, 78, 364-369.

Picard, A., Gartman, A., Clarke, D.R., and Girguis, P.R. (2018) Sulfate-reducing bacteria influence the nucleation and growth of mackinawite and greigite. Geochim Cosmochim Acta 220: 367-384.

Pósfai, M., and Dunin-Borkowski, R.E. (2006) Sulfides in biosystems. Rev Mineral Geochem 61: 679 - 714.

Rabus, R., Hansen, T.A., and Widdel, F. (2013) Dissimilatory sulfate- and sulfur-reducing prokaryotes. In The Prokaryotes. Rosenberg, E., Delong, E.F., Lory, S., Stackebrandt, E., and F. Thompson. Heidelberg: Springer, , pp. 309-404

Rickard, D., and Morse, J.W. (2005) Acid volatile sulfide (AVS). Mar Chem 97: 141 - 197.

Rickard, D., and Luther III, G.W. (2007) Chemistry of iron sulfides. Chem Rev 107: 514-562.

Sánchez-Andrea, I., Rodriguez, N., Amils, R., and Sanz, J.L. (2011) Microbial diversity in anaerobic sediments at Rio Tinto, a naturally acidic environment with a high heavy metal content. Appl Environ Microbiol 77: 6085-6093.

Sánchez-Andrea, I., Stams, A.J.M., Amils, R., and Sanz, J.L. (2013) Enrichment and isolation of acidophilic sulfate-reducing bacteria from Tinto River sediments. Environ Microbiol Rep 5: 672-678.

Sánchez-Andrea, I., Sanza, J.L., Bijmans, M.F.M., and Stams, A.J.M. (2014) Sulfate reduction at low pH to remediate acid mine drainage. J Hazard Mat 269: 98-109.

Sánchez-Andrea, I., Stams, A.J.M., Hedrich, S., Ňancucheo, I., and Johnson, D.B. (2015) *Desulfosporosinus acididurans* sp. nov.: an acidophilic sulfate-reducing bacterium isolated from acidic sediments. Extremophiles 19: 39-47.

Sánchez-España, J., Yusta, I., and Burgos, W.D. (2016a) Geochemistry of dissolved aluminum at low pH: Hydrobasaluminite formation and interaction with trace metals, silica and microbial cells under anoxic conditions. Chem Geol 441: 124-137.

Sánchez-España, J., Yusta, I., Gray, J., and Burgos, W.D. (2016b) Geochemistry of dissolved aluminum at low pH: Extent and significance of Al–Fe(III) coprecipitation below pH 4.0. Geochim Cosmochim Acta 175: 128-149.

Santra, M.K., and Panda, D. (2007) Acid-induced loss of functional properties of bacterial cell division protein FtsZ: Evidence for an alternative conformation at acidic pH. Proteins Struct Funct Bioinf 67: 177-188.

Sen, A.M., and Johnson, D.B. (1999) Acidophilic sulphate-reducing bacteria: candidates for bioremediation of acid mine drainage. In Biohydrometallurgy and the Environment Toward

the Mining of the 21st Century, Process Metallurgy 9. Amils, R., and A. Ballester (eds). Amsterdam: Elsevier, pp. 709-718.

Senko, J.M., Zhang, G., McDonough, J.T., Bruns, M.A., and Burgos, W.D. (2009) Metal reduction at low pH by a *Desulfosporosinus* species: Implications for the biological treatment of acidic mine drainage. Geomicrobiology J 26: 71-82.

Sheoran, A.S., Sheoran, V., and Choudhary, R.P. (2010) Bioremediation of acid-rock drainage by sulphate-reducing prokaryotes: A review. Miner Eng 14: 1073-1100.

Slonczewski, J.L., Fujisawa, M., Dopson, M., and Krulwich, T.A. (2009) Cytoplasmic pH measurement and homeostasis in bacteria and archaea. Adv Microb Physiol 55: 1–79.

Wendt-Potthoff, K., and Neu, T.R. (1998) Microbial processes for potential in situ remediation of acidic lakes. In Acid Mining Lakes - Acid Mine Drainage, Limnology and Reclamation. Geller, W., H. Klapper and W. Salomons (eds). Berlin: Environmental Science Series, Springer, pp. 269-284.

White, C., and Gadd, G.M. (1998) Accumulation and effects of cadmium on sulphate-reducing bacterial biofilms. Microbiology 144: 1407-1415.

White, C., and Gadd, G.M. (2000) Copper accumulation by sulfate-reducing bacterial biofilms. FEMS Microbiol Lett 183: 313-318.

Widdel, F., and Bak, F. (1992) Gram-negative mesophilic sulfate-reducing bacteria. In The Prokaryotes. Balows, A., Trüper, H.G., Dworkin, M., Harder, W., and Schleifer, H. (eds). Berlin: Springer, pp. 3352-3389.

Wolthers, M., Van der Gaast, S.J., and Rickard, D. (2003) The structure of disordered mackinawite. American Mineralogist 88: 2007-2015.

Wolthers, M., Charlet, L., Van der Linde, P.R., Rickard, D., and Van der Weijden, C.H. (2005) Surface chemistry of disordered mackinawite (FeS). Geochim Cosmochim Acta 69: 3469-3481.

Yang, Y., Wikieł, A.J., Dall'Agnol, L.T., Eloy, P., Genet, M.J., Moura, J.J.G, et al. (2016) Proteins dominate in the surface layers formed on materials exposed to extracellular polymeric substances from bacterial cultures. Biofouling 32: 95-108.

Zhang, Z., Schwartz, S., Wagner, L., and Miller, W. (2000) A greedy algorithm for aligning DNA sequences. J Comput Biol 7: 203-214.

Zinkevich, V., Bogdarina, I., Kang, H., Hill, M.A.W., Tapper, R., and Beech, I.B. (1996) Characterisation of exopolymers produced by different isolates of marine sulphate-reducing bacteria. Int Biodeterior Biodegradation 37: 163-172.

Figure legends

Fig. 1: Growth characteristics of strain 3baa in relation to the initial pH of the medium (pH_{ini}) with sulfate reduction rates (SRR) and total amount of sulfate reduced during incubation (A), cell numbers of the culture liquid in the stationary phase (B), pH values at which main sulfate reduction started and pH values at the end of incubation (linear regression as dashed line; pH = pH_{ini} as dotted line) (C), lapse of time until main sulfate reduction started ('Lag phase SR') (D). SRRs correspond to slope coefficients of linear regression lines with bars indicating standard error. Cell numbers are given as mean of four counts with bars indicating standard deviation. All other values are displayed as mean of duplicate samples with bars indicating min. and max. values. For cultures at pH_{ini} 2.6 and 3.1, results from the duplicate samples of first series and from the one replicate of second series are shown separately. Lag phase SR is only shown for the second series.

Fig. 2: Growth of strain 3baa in the culture liquid at pH_{ini} 3.2 with logarithmized cell numbers (A), pH and sulfate concentration (B), concentrations of the dissolved elements Al and Fe (C), and cell length (D) as a function of time. Results are displayed as mean of duplicate or quadruplicate (day 28) samples with bars indicating min. and max. values or standard deviation (day 28).

Fig. 3: CLSM images of biofilms from day 28 (A – C) and day 49 (D – M). Images are displayed as maximum intensity projection (MIP) along Z direction from the overlay of all channels (A, D, I) and separately for the green channel (nucleic acid stain) (B, E, J), the red channel (protein stain) (C, F, K), and the white channel (reflection) (H, M). MIPs along Y direction from the overlay of all channels (G, L). Images were taken from segment 1-2 on day 28 (A – C) and segments 3-4 (D – H) and 2-3 on day 49 (I – M). Scale bar = 20 µm.

Fig. 4: SEM images of biofilms showing cell and mineral precipitates in segment 1-2 on day 38 (A, B) and segments 1-2 (C, D) and 4-5 on day 49 (E, F). During an early stage of biofilm formation an Al-rich surface layer and Al-rich globules were observed (A, B), at a later stage precipitates rich in Fe and S were observed either shaped as ‘flakes’ (C) or as ‘crosses’ and ‘stars’ (E, F). At this later stage many cells become heavily coated with Al-rich globules (D).

Fig. 5: TEM images showing a cross section through the biofilm with several cells and mineral precipitates (A) and through a single cell with Al-rich globules attached to the cell surface (B). OM: outer membrane; IM: inner membrane; arrow: indicates a middle layer between the two membranes.

Fig. 6: Phylogenetic tree based on 16S-rRNA gene sequences of strain 3baa, related clones, and type species of sulfate reducers of the Firmicutes. The Neighbour Joining method was used as cluster algorithm. Bootstrap values are indicated on corresponding branches. Scale bar indicates the number of nucleotide substitutions per site.

Fig. 7: Sequence of biofilm formation: sulfate reduction by planktonic cells at low rates starting at pH ≥2.5 (A), precipitation of Al hydroxides at pH ≥3.5 (B), attachment and growth of bacterial cells on solid surface facilitated by ionic bonding with Al hydroxides (C), precipitation of Fe sulfides at pH ≥4.5 and further biofilm growth leading to increasing sulfate reduction rates (D).

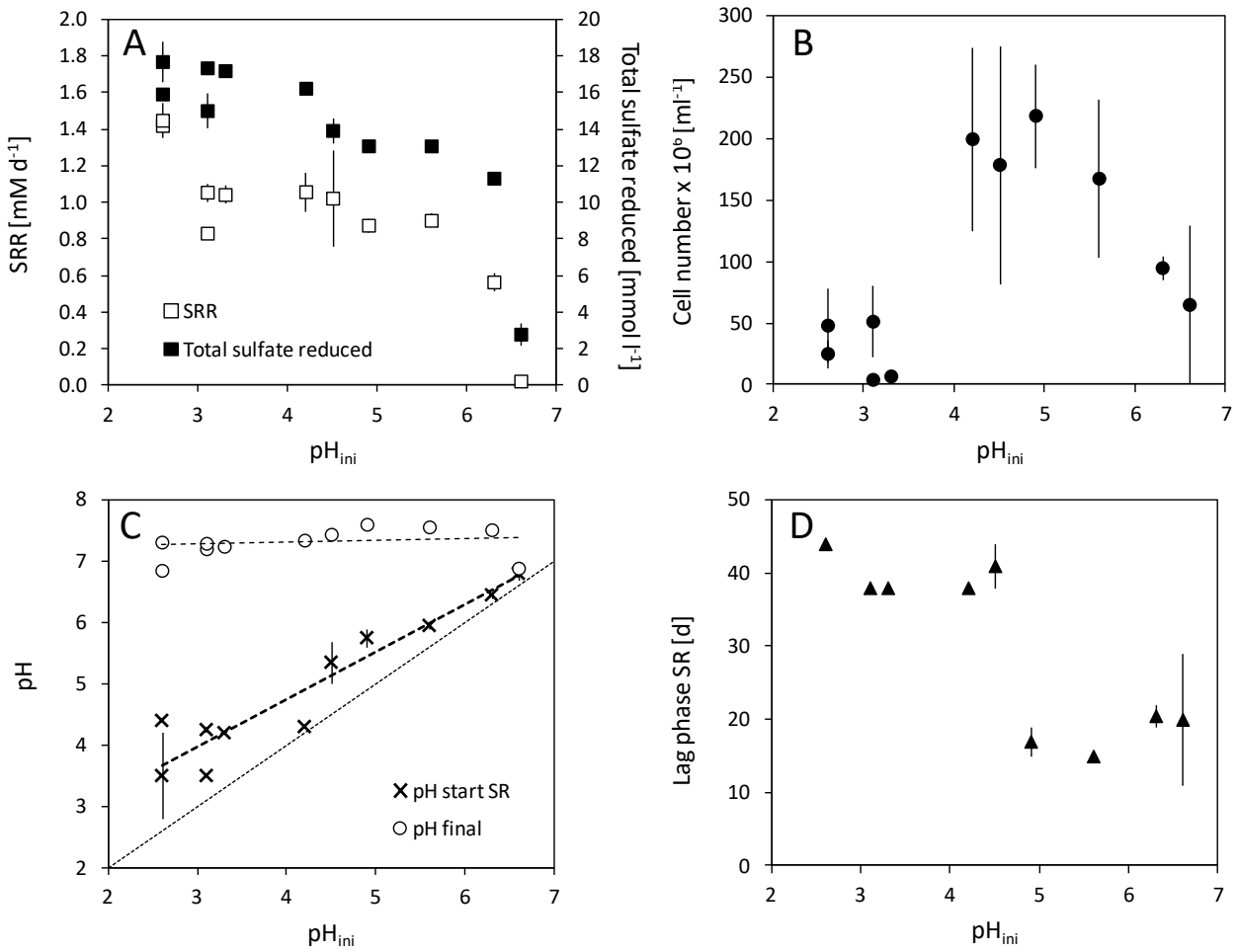

Fig. 1

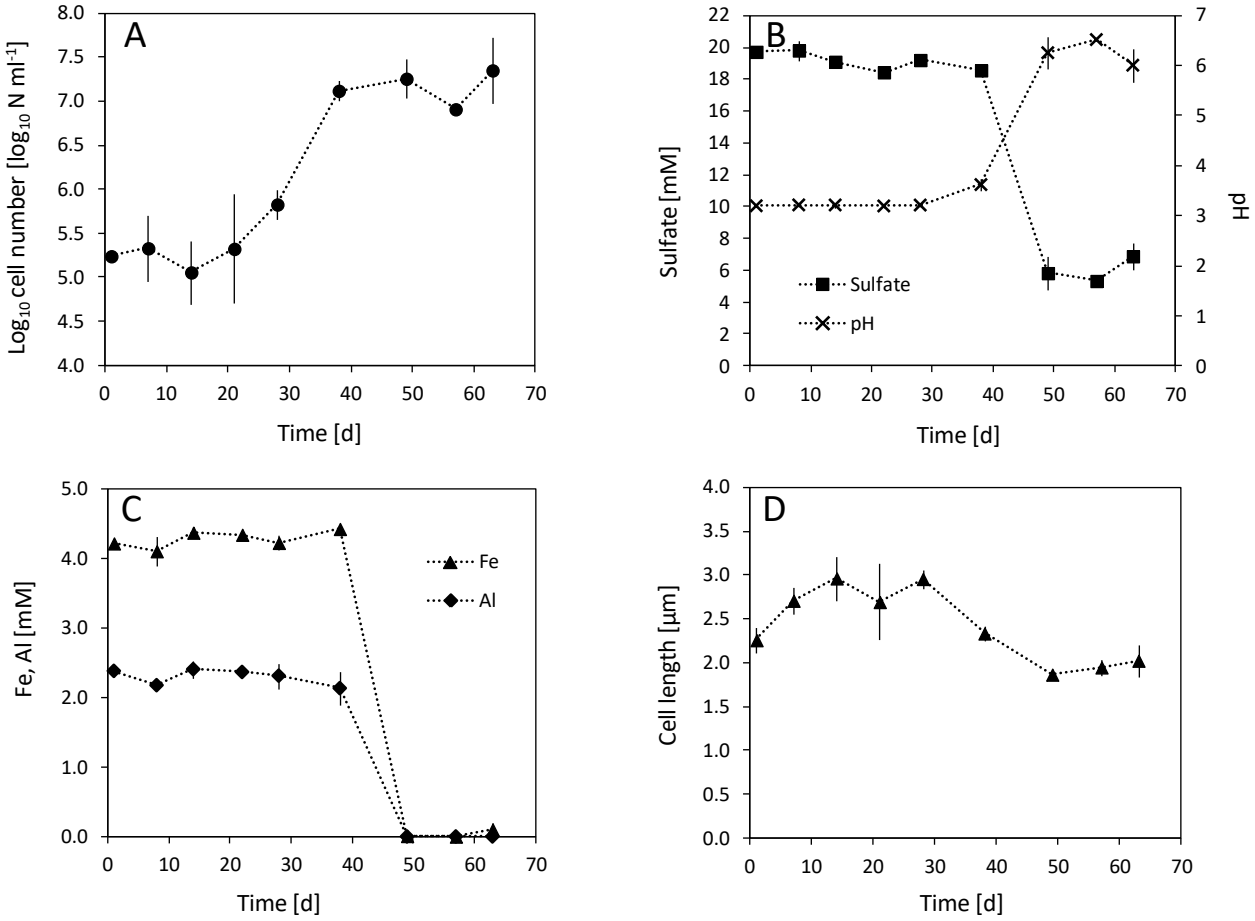

Fig. 2

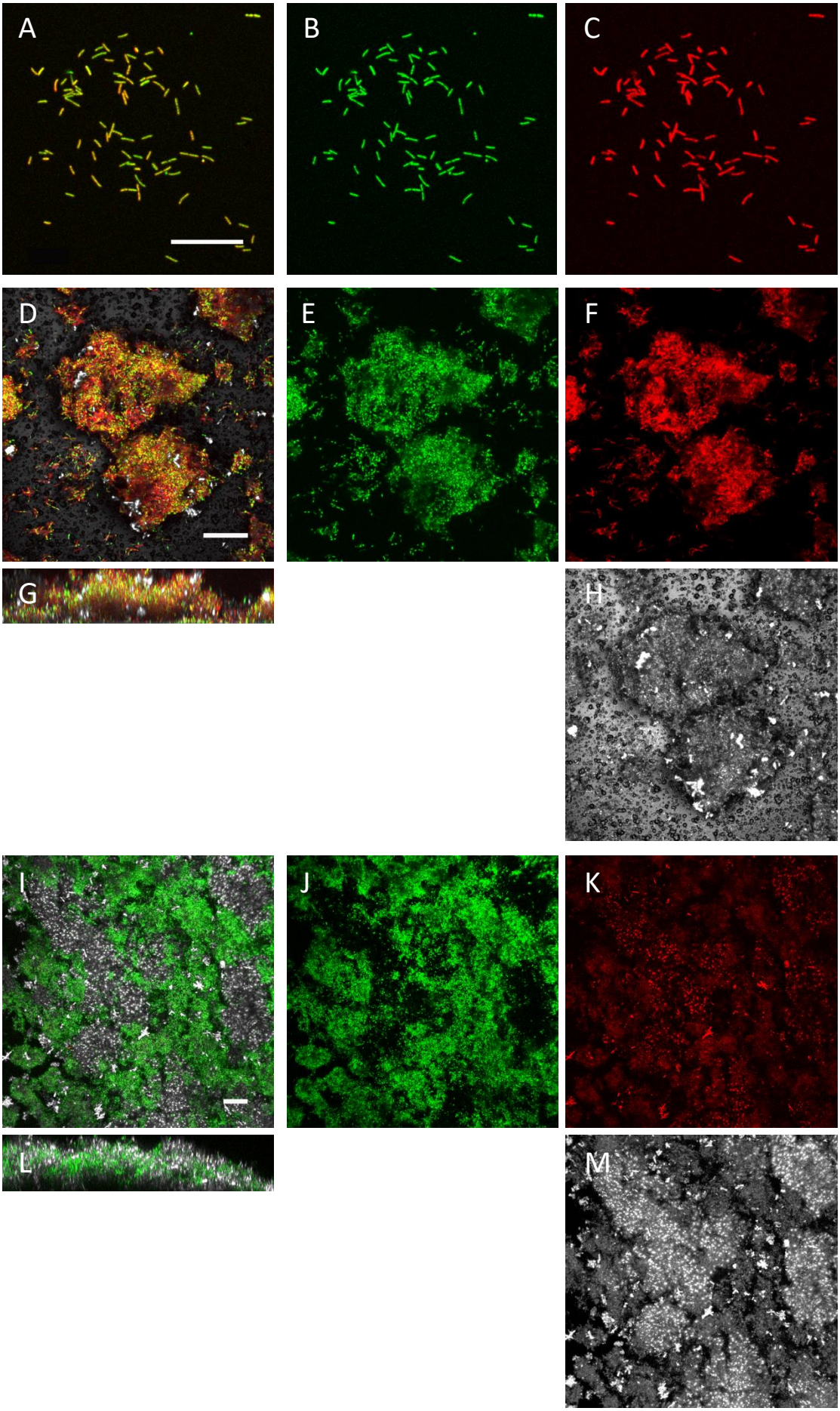

Fig. 3

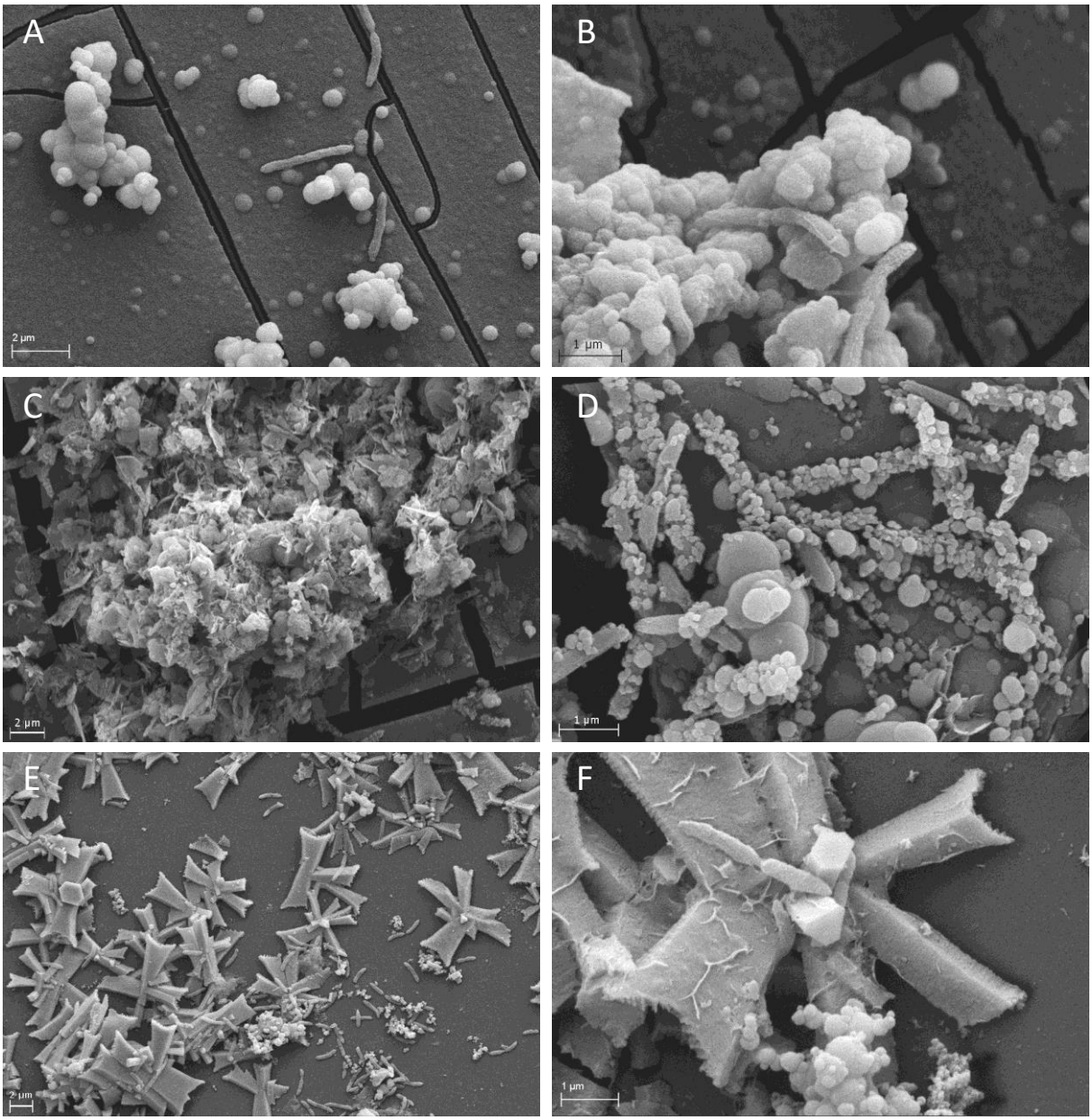

Fig. 4

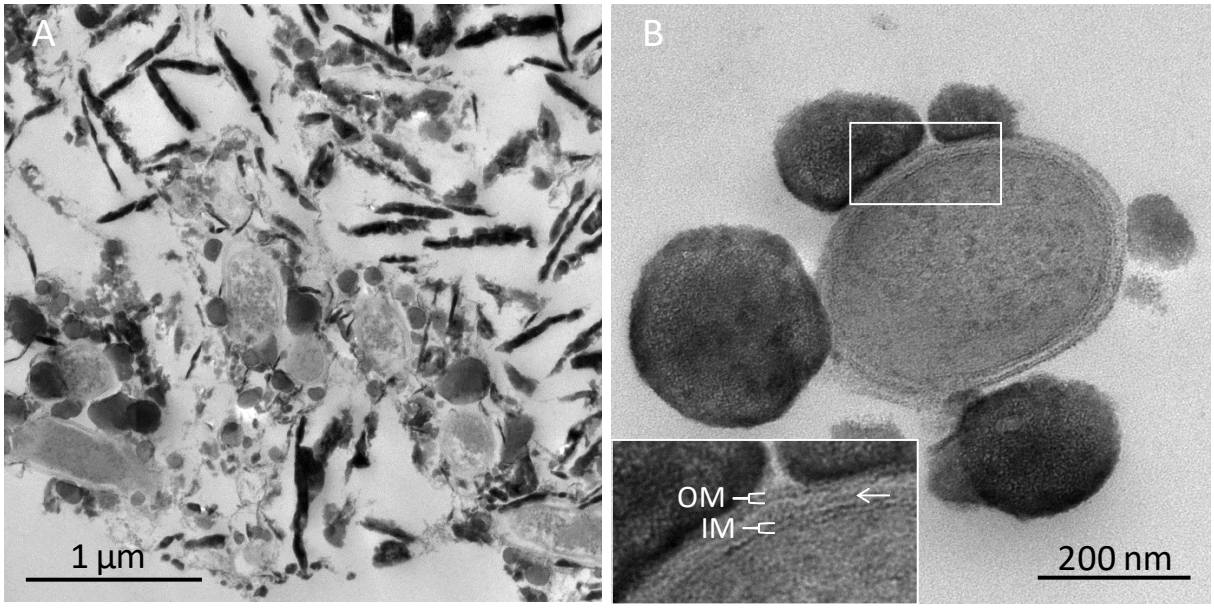

Fig. 5

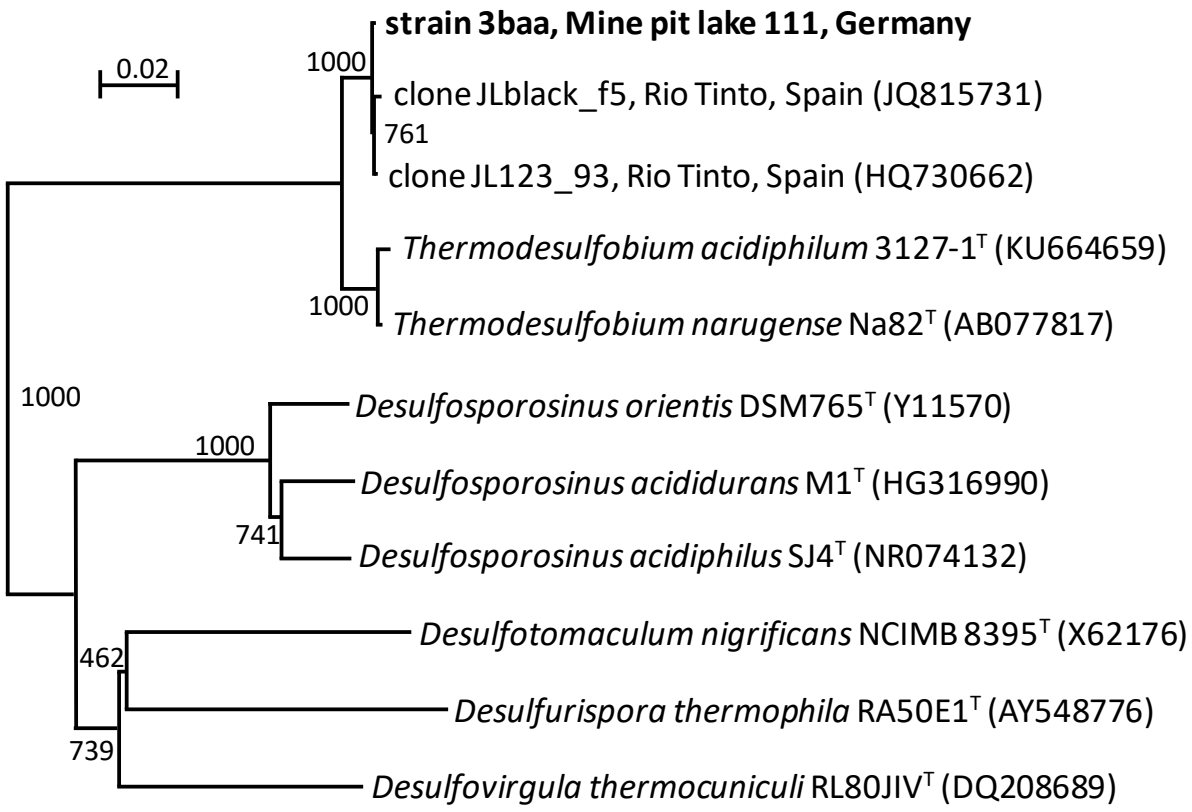

Fig. 6

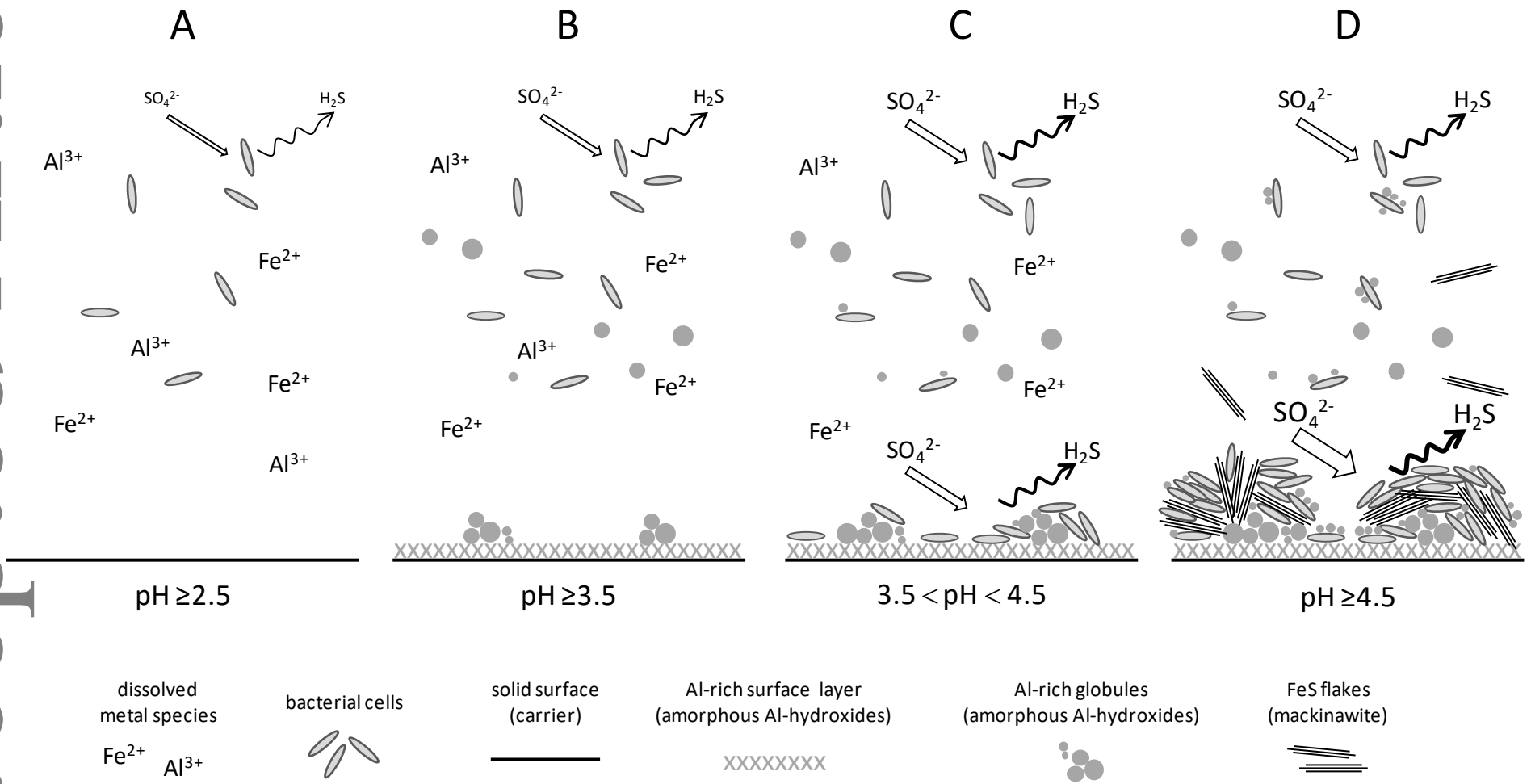

Fig. 7